

# Realizing Multi-Point Vehicular Positioning via Millimeter-wave Transmission

Zezhong Zhang\*, Seung-Woo Ko<sup>†</sup>, Rui Wang<sup>‡</sup>, and Kaibin Huang\*

\*Department of Electrical and Electronic Engineering, The University of Hong Kong

<sup>†</sup>Division of Electronics and Electrical Information Engineering, Korea Maritime and Ocean University

<sup>‡</sup>Department of Electrical and Electronic Engineering, Southern University of Science and Technology

Email: zzzhang@eee.hku.hk, swko@kmou.ac.kr, wang.r@sustech.edu.cn, huangkb@eee.hku.hk

**Abstract**—Multi-point detection of the full-scale environment is an important issue in autonomous driving. The state-of-the-art positioning technologies (such as RADAR and LIDAR) are incapable of real-time detection without line-of-sight. To address this issue, this paper presents a novel multi-point vehicular positioning technology via millimeter-wave (mmWave) transmission that exploits multi-path reflection from a *target vehicle* (TV) to a *sensing vehicle* (SV), which enables the SV to fast capture both the shape and location information of the TV in *non-line-of-sight* (NLoS) under the assistance of multi-path reflections. A *phase-difference-of-arrival* (PDoA) based hyperbolic positioning algorithm is designed to achieve the synchronization between the TV and SV. The *stepped-frequency-continuous-wave* (SFCW) is utilized as signals for multi-point detection of the TVs. Transceiver separation enables our approach to work in NLoS conditions and achieve much lower latency compared with conventional positioning techniques.

## I. INTRODUCTION

Autonomous driving has grown into a reality with rapid progress of diverse technologies [1]. Much effort and investment have been devoted by top automobile companies (Tesla, BMW) and Internet companies (Google, Baidu), leading to significant achievements toward commercialization. One remaining challenge to attain full autonomous driving is to accurately recognize vehicles nearby, termed *vehicular positioning* [2]. Compared to conventional single-point positioning approaches [3], [4], vehicular positioning is required to accurately estimate high-resolution positioning information including location, size, and shape of *target vehicle* (TV). We call it *multi-point vehicular positioning* in this paper.

### A. Positioning

Single-point positioning has been widely used in the area of mobile positioning, which determines the object's position as a single point since a mobile device is typically small enough to mark a representative point. The most common way is to use a built-in *Global Positioning System* (GPS) receiver but its usage is limited since GPS signals are frequently blocked in urban environments. On the other hand, single-point positioning is unsuitable for autonomous driving due to the fact that a vehicle is too big to represent a single point. The lack of shape and size information may cause fatal accidents [10]. One can claim to be able to deliver shape and size information separately through a reliable communication link but it needs additional efforts to align them with the estimated point perfectly.

To overcome the limitation of single-point positioning, there have been efforts in the area of multi-point positioning. Passive multi-point positioning detects the natural radiation from the target objects without emitting discernible radiations. Infrared sensors and cameras are representative ones, which easily retrieve the positioning information in a fully covert manner [11]. On the other hand, *active multi-point positioning* techniques illuminate the target and detect its position with data extracted from reflected signals or lights [11], [12]. A *Radio-Detection-And-Ranging* (RADAR) system is the most popular one in surface and subsurface detections, which is implemented by impulse waveforms and *continuous-waves* (CWs) with different frequency modulations [13]. *Light-Detection-And-Ranging* (LIDAR), another new emerging active positioning technique, utilizes narrow laser beams for positioning and uses the scanning mirror for fast scanning [17].

More importantly, a fatal drawback of the above techniques is that they are only capable of detecting the vehicles in LoS since the corresponding mediums cannot penetrate a large solid blockage in the road such as a truck or a bus. However, the disability of detection in NLoS results in severe safety issues because many car accidents happen when the drivers are unaware of the environment. Therefore, designing techniques for positioning in NLoS is an urgent task for applications of autonomous driving in real-life. In [19], a NLoS positioning technique is developed to estimate a vehicle's position by exploiting the geometry information of multi-path signal transmissions. It is also possible to infer the vehicle's size and shape if the vehicle equips multiple antenna clusters, but the resultant resolution is low.

### B. Main Contributions

The contributions of this work are summarized as follows.

- 1) **Real-time Positioning:** The proposed multi-point vehicular positioning is a one-way simultaneous multi-antenna transmissions from the TV to the SV. Compared to conventional multi-point positioning techniques requiring time-consuming scanning process, our technique is able to achieve ultra-low latency and realize real-time multi-point positioning.
- 2) **Synchronization:** In the above one-way simultaneous transmission system, a prerequisite for the multi-point positioning is to know a clock synchronization gap between the SV and the TV. To this end, we design a novel synchronization algorithm

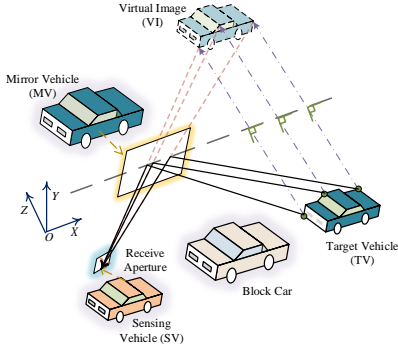


Figure 1: Illustration of signals reflection by mirror vehicles.

based on multiple *Phase-Difference-of-Arrival* (PDoA) information obtained by transmitting *signature waveforms* (SWs) from representative antennas. The PDoA information leads to constructing a system of equations following a hyperbolic geometry.

3) **Positioning in LoS and NLoS:** In LoS case, A FFT-based signal processing technique is used to retrieve the location information of all transmit antennas, i.e., the TV's position, based on the received signals. In NLoS, the SV uses multiple *mirror vehicles* (MVs) as reflectors of the TV's transmitted mmWave signal to estimate the TV's position. By the aid of specular reflection, the SV is able to achieve the NLoS TV's multi-point positioning if the MV's locations are given but unknown in practice. This difficulty is overcome by exploiting the geometry relation between the vehicle's reflected and *real positions* (RPs).

## II. SYSTEM MODEL

Consider the scenario with multiple vehicles located on the road. Each vehicle is equipped with an antenna array around the vehicle body, which can generally represent its shape. We adopt the wide-band positioning system using *stepped-frequency-continuous-wave* (SFCW) [13] at mmWave spectrums as a waveform for each transmit antenna. It comprises multiple CW signals with different frequencies, each of which is separated by a certain amount.

In mmWave bands, due to high attenuation loss and sparse distribution of scatters, most signal propagations follow LoS especially when vehicles are dispersive. However, a vehicle's metal body with a favorable reflection property makes it possible to propagate signals even in NLoS. Fig. 1 graphically illustrates the above property such that the SV tries to detect a TV by receiving the TVs' signals, but the SV is blocked by other vehicles and cannot see the TV directly. One alternative is to exploit nearby MVs as reflectors of the signals. With multiple MVs, the SV is able to obtain the position of the TV. Without loss of generality, we assume that the receive aperture is located at the SV's left side, and  $X$ ,  $Y$ , and  $Z$ -axes represent its moving direction, height, and width, respectively.

### A. Signal Model

Two types of TV transmissions are considered depending on different purposes. The first is the SFCW transmission enabling to obtain TV's position at the SV, and the second is a *signature waveform* (SW) transmission [24] to compensate the SV-TV synchronization gap.

1) *SFCW Transmission:* All TV's antennas simultaneously broadcast the same SFCW waveform denoted by  $s(t)$  as

$$s(t) = [\exp(j2\pi f_1 t), \dots, \exp(j2\pi f_K t)]^T, \quad (1)$$

where  $\{f_k\}_{k=1}^K$  represents the set of frequencies with constant gap  $\Delta$  such that  $f_k = f_1 + (k-1)\Delta$  for  $k = 1, \dots, K$ . The received signal at the SV's antenna  $m$  is given as

$$\mathbf{r}_m(t) = \sum_{\ell=0}^L \mathbf{r}_m^{(\ell)}(t), \quad (2)$$

where  $\mathbf{r}_m^{(\ell)}(t)$  denotes the signal reflected by the  $\ell$ -th MV as

$$\mathbf{r}_m^{(\ell)}(t) = \Gamma^{(\ell)} \sum_{n=1}^N \mathbf{r}_{n,m}^{(\ell)}(t) = \Gamma^{(\ell)} \sum_{n=1}^N \mathbf{s}(t + \sigma - \tau_{n,m}^{(\ell)}). \quad (3)$$

Here,  $\Gamma^{(\ell)}$  is the complex reflection coefficient given as  $\Gamma^{(\ell)} = |\Gamma^{(\ell)}| \exp(j\angle\Gamma^{(\ell)})$ <sup>1</sup>,  $N$  is the number of TV's antennas,  $\sigma$  is the TV-SV synchronization gap (in sec), and  $\tau_{n,m}^{(\ell)}$  is the signal travel time from TV's antenna  $n$  to SV's antenna  $m$  proportional to the propagation distance  $d_{n,m}$ , i.e.,  $d_{n,m} = c \cdot \tau_{n,m}^{(\ell)}$  where  $c = 3 \cdot 10^8$  (m/sec) is the speed of light. Note that signal path  $\ell = 0$  represents the LoS path of which the reflection coefficient  $\Gamma^{(0)}$  is one. Last, we assume that the signals reflected by different MVs come from different directions, facilitating to differentiate signals from different MVs according to the *angle-of-arrival* (AoA). In other words, we can decompose (2) into individual  $\mathbf{r}_m^{(\ell)}(t)$  as

$$\mathbf{R}_m(t) = [\mathbf{r}_m^{(0)}(t), \mathbf{r}_m^{(1)}(t), \dots, \mathbf{r}_m^{(L)}(t)]. \quad (4)$$

The synchronization gap  $\sigma$  is an unknown parameter the SV attempts to estimate. Assuming the estimated gap is  $\tilde{\sigma}$ , the received signal (4) is demodulated by multiplying  $\mathbf{D} = \text{diag}\{s(t + \tilde{\sigma})^H\}$

$$\mathbf{Y}_m = [\mathbf{y}_m^{(0)}, \mathbf{y}_m^{(1)}, \dots, \mathbf{y}_m^{(L)}] = \mathbf{D}\mathbf{R}_m(t), \quad (5)$$

where  $\mathbf{y}_m^{(\ell)} = \mathbf{D}\mathbf{r}_m^{(\ell)}(t) = [y_m^{\ell,1}, y_m^{\ell,2}, \dots, y_m^{\ell,K}]^T$  with

$$y_m^{\ell,k} = \Gamma^{(\ell)} \sum_{n=1}^N \exp[j2\pi f_k(\sigma - \tilde{\sigma} - \tau_{n,m}^{(\ell)})]. \quad (6)$$

<sup>1</sup>The reflection planes are sides of vehicles, which are usually plane and smooth. In addition, the limited size of the receive aperture makes the incident angles of the signals almost the same. As a result, the  $\Gamma^{(\ell)}$  can be well approximated as a constant regardless of antennas (see e.g., [13], [25]).

2) *SW Transmission*: Two representative antennas, a and b, are selected in the array of the TV with coordinates  $\mathbf{x}_a = (x_a, y_a, z_a)$  and  $\mathbf{x}_b = (x_b, y_b, z_b)$ , respectively. To estimate  $\mathbf{x}_a$  and  $\mathbf{x}_b$  as an intermediate step for the synchronization, each of them simultaneously transmits SWs comprising two CWs with different frequencies as

$$\begin{aligned} \mathbf{s}_a(t) &= [\exp(j2\pi f_a t), \exp(j2\pi(f_a + \Delta)t)]^T, \\ \mathbf{s}_b(t) &= [\exp(j2\pi f_b t), \exp(j2\pi(f_b + \Delta)t)]^T, \end{aligned} \quad (7)$$

where  $f_a$  and  $f_b$  represent the SWs' frequencies originated from the antennas a and b respectively, and  $\Delta$  is the frequency separation for another CW in each SW. The frequency bands for the SWs do not overlap to each other and are different from that of the SFCW, namely,  $f_a < f_a + \Delta < f_b < f_b + \Delta < f_1$ , enabling to receive and demodulate the SWs independently from the SFCW without interference. Similar to (4), the received signals at the SV's antenna  $m$  are expressed as

$$\mathbf{A}_m(t) = [\mathbf{a}_m^{(1)}(t), \dots, \mathbf{a}_m^{(L)}(t)], \mathbf{B}_m(t) = [\mathbf{b}_m^{(1)}(t), \dots, \mathbf{b}_m^{(L)}(t)],$$

where  $\mathbf{a}_m^{(\ell)}(t) = \Gamma^{(\ell)} \mathbf{s}_a(t + \sigma - \tau_{a,m}^{(\ell)})$  and  $\mathbf{b}_m^{(\ell)}(t) = \Gamma^{(\ell)} \mathbf{s}_b(t + \sigma - \tau_{b,m}^{(\ell)})$ . By multiplying  $\mathbf{D}_a = \text{diag}\{\mathbf{s}_a(t)^H\}$  and  $\mathbf{D}_b = \text{diag}\{\mathbf{s}_b(t)^H\}$  respectively,  $\mathbf{A}_m(t)$  and  $\mathbf{B}_m(t)$  can be demodulated as  $\mathbf{D}_a \mathbf{A}_m(t) = [\boldsymbol{\alpha}_m^{(0)}, \boldsymbol{\alpha}_m^{(1)}, \dots, \boldsymbol{\alpha}_m^{(L)}]$  and  $\mathbf{D}_b \mathbf{B}_m(t) = [\boldsymbol{\beta}_m^{(0)}, \boldsymbol{\beta}_m^{(1)}, \dots, \boldsymbol{\beta}_m^{(L)}]$ , where

$$\begin{aligned} \boldsymbol{\alpha}_m^{(\ell)} &= \Gamma^{(\ell)} \left[ \exp(j2\pi f_a(\sigma - \tau_{a,m}^{(\ell)})), \exp(j2\pi(f_a + \Delta)(\sigma - \tau_{a,m}^{(\ell)})) \right], \\ \boldsymbol{\beta}_m^{(\ell)} &= \Gamma^{(\ell)} \left[ \exp(j2\pi f_b(\sigma - \tau_{b,m}^{(\ell)})), \exp(j2\pi(f_b + \Delta)(\sigma - \tau_{b,m}^{(\ell)})) \right]. \end{aligned}$$

### B. Problem Formulations

To establish the direct relation between the propagation distance and the phase extracted from  $y_m^{\ell,k}$  (6), the SV aims at compensating the clock synchronization gap  $\sigma$ , namely,

$$\bigcup_{\ell=1}^L \{\boldsymbol{\alpha}_m^{(\ell)}, \boldsymbol{\beta}_m^{(\ell)}\}_{m=1}^M \implies \tilde{\sigma} = \sigma, \quad (\text{E1})$$

where  $M$  is the number of receive antennas deployed in the SV. Assume that the synchronization is made. The  $y_m^{\ell,k}$  (6) is then rewritten by the following surface integral form:

$$y_m^{\ell,k} \underset{(\sigma=\tilde{\sigma})}{\implies} \Gamma^{(\ell)} \int \mathbf{1}_{\mathbf{x}^{(\ell)}} \exp\left(-j2\pi \frac{f_k}{c} D(\mathbf{x}, \mathbf{p}_m)\right) d\mathbf{x}, \quad (8)$$

where  $\mathbf{1}_{\mathbf{x}^{(\ell)}}$  is an indicator to become one if a TX antenna exists on point  $\mathbf{x}$ , which is symmetric to the point  $\mathbf{x}^{(\ell)}$  w.r.t. the surface of MV  $\ell$ , and zero otherwise, and  $D(\mathbf{x}, \mathbf{p}_m)$  represent the total propagation distance between  $\mathbf{x}$  and the location of RX antenna  $m$  denoted by  $\mathbf{p}_m$ . Estimating  $\{\mathbf{1}_{\mathbf{x}^{(\ell)}}\}$  is equivalent to detecting TV's position  $\ell$ , namely,

$$\bigcup_{k=1}^K \bigcup_{m=1}^M y_m^{\ell,k} \implies \{\mathbf{1}_{\mathbf{x}^{(\ell)}}\}. \quad (\text{E2})$$

It is worth noting that in case of LoS path ( $\ell = 0$ ), the distance  $D(\mathbf{x}, \mathbf{p}_m)$  is the direct distance between  $\mathbf{x}$  and  $\mathbf{p}_m$ . Thus, the position of real TV is directly detected. In NLoS case,

$D(\mathbf{x}, \mathbf{p}_m)$  corresponds to the total distance from  $\mathbf{x}$  via MV  $\ell$  to  $\mathbf{p}_m$ . Since SV has no priori information of MV's location, the detected position could be different from the RP due to reflection, which is called a *virtual position* (VP) (see Fig. 1). It is necessary to map multiple VPs into the RP, namely,

$$\bigcup_{\ell=0}^L \{\mathbf{1}_{\mathbf{x}^{(\ell)}}\} \implies \{\mathbf{1}_{\mathbf{x}}\}. \quad (\text{E3})$$

## III. MULTI-POINT VEHICULAR POSITIONING

In this section, we consider a case where a LoS path between the TV and the SV exists, making it reasonable to ignore other NLoS paths due to the significant power difference between LoS and NLoS paths. Thus only synchronization and multi-point positioning steps are needed, which are explained in detail, following overview, algorithm description and performance analysis.

### A. Synchronization

1) *Overview*: We apply the technique of *phase-difference-of-arrival* (PDoA) based localization [27] to compensate the synchronization gap, which is illustrated in the following. Consider the SWs from the representative antenna a first. The received SWs at the receive antenna  $m$  through the signal path reflected by the  $\ell$ -th MV are given as

$$\boldsymbol{\alpha}_m^{(\ell)} = \Gamma^{(\ell)} \left[ \exp(j2\pi f_a(\sigma - \tau_m^{(\ell)})), \exp(j2\pi(f_a + \Delta)(\sigma - \tau_m^{(\ell)})) \right],$$

where  $\tau_m^{(\ell)}$  represents the flight time, and the indices of the transmit antennas are omitted for brevity. At the SV's antenna  $m$ , the phase difference between the two components is calculated as  $\eta_m^{(\ell)} = 2\pi\Delta(\tau_m^{(\ell)} - \sigma)$ . Note that  $\sigma$  is the same for signals from different paths. Recalling the relation between the propagation distance  $d_m^{(\ell)}$  and  $\tau_m^{(\ell)}$ , i.e.,  $d_m^{(\ell)} = \tau_m^{(\ell)} \cdot c$  with light speed  $c$ , the synchronization gap  $\sigma$  is given as

$$\sigma = \tau_m^{(\ell)} - \frac{\eta_m^{(\ell)}}{2\pi\Delta} = \frac{d_m^{(\ell)}}{c} - \frac{\eta_m^{(\ell)}}{2\pi\Delta}. \quad (9)$$

Moreover, according to the geometric relation between the  $\ell$ -th VP and the TV shown in Fig. 1, the propagation distance can be presented as  $d_m^{(\ell)} = \|\mathbf{p}_m - \mathbf{x}_a^{(\ell)}\|$ , where  $\mathbf{x}_a^{(\ell)}$  is the location of the antenna a on the VP  $\ell$ , which are different from the real location denoted by  $\mathbf{x}_a$  in case of NLoS. Because the locations of all SV's antennas  $\{\mathbf{p}_m\}$  are given, the synchronization problem is translated to find the location  $\mathbf{x}_a^{(\ell)} = (x_a^{(\ell)}, y_a^{(\ell)}, z_a^{(\ell)})$ . Specifically, let  $F_i(\mathbf{x}_n^{(\ell)})$  denote the propagation distance difference from the antenna  $n$  on the VP  $\ell$  to the SV's antennas  $m$  and 1 as

$$\begin{aligned} F_m(\mathbf{x}_a^{(\ell)}) &= \left\| \mathbf{p}_m - \mathbf{x}_a^{(\ell)} \right\| - \left\| \mathbf{p}_1 - \mathbf{x}_a^{(\ell)} \right\| \\ &= d_m^{(\ell)} - d_1^{(\ell)} \stackrel{(a)}{=} c \frac{(\eta_m^{(\ell)} - \eta_1^{(\ell)})}{2\pi\Delta}, \quad m=2, \dots, M, \end{aligned} \quad (10)$$

where (a) follows from (9). In (10), there are  $M - 1$  equations with three unknowns  $x_a^{(\ell)}$ ,  $y_a^{(\ell)}$ , and  $z_a^{(\ell)}$ .

2) *Algorithm Description*: One challenge to solve (10) is a nonlinearity of  $F_m(\mathbf{x}_a^{(\ell)})$  following a hyperbolic geometry. To overcome the difficulty, we use the Gauss-Newton method [28]. Assume that the initial value  $\tilde{\mathbf{x}}_a^{(\ell)}$  is a good estimator of  $\mathbf{x}_a^{(\ell)}$ . Then,  $F_m(\mathbf{x}_a^{(\ell)})$  can be approximated as

$$F_m(\mathbf{x}_a^{(\ell)}) \approx F_m(\tilde{\mathbf{x}}_a^{(\ell)}) + \frac{\partial F_m(\tilde{\mathbf{x}}_a^{(\ell)})}{\partial \mathbf{x}_a^{(\ell)}} \mathbf{h}, \quad (11)$$

where  $\mathbf{h} = [h_x, h_y, h_z]^T$ . Plugging (11) into (10) gives the following linear of equations:

$$\mathbf{G}(\tilde{\mathbf{x}}_a^{(\ell)}) \mathbf{h} = \mathbf{b}(\tilde{\mathbf{x}}_a^{(\ell)}), \quad (\text{E4})$$

where

$$\mathbf{G}(\tilde{\mathbf{x}}_a^{(\ell)}) = \begin{bmatrix} \frac{\partial F_2(\tilde{\mathbf{x}}_a^{(\ell)})}{\partial x_a^{(\ell)}} & \frac{\partial F_2(\tilde{\mathbf{x}}_a^{(\ell)})}{\partial y_a^{(\ell)}} & \frac{\partial F_2(\tilde{\mathbf{x}}_a^{(\ell)})}{\partial z_a^{(\ell)}} \\ \dots & \dots & \dots \\ \frac{\partial F_M(\tilde{\mathbf{x}}_a^{(\ell)})}{\partial x_a^{(\ell)}} & \frac{\partial F_M(\tilde{\mathbf{x}}_a^{(\ell)})}{\partial y_a^{(\ell)}} & \frac{\partial F_M(\tilde{\mathbf{x}}_a^{(\ell)})}{\partial z_a^{(\ell)}} \end{bmatrix}, \quad (12)$$

$$\mathbf{b}(\tilde{\mathbf{x}}_a^{(\ell)}) = \begin{bmatrix} c \frac{(\eta_2 - \eta_1)}{2\pi\Delta} - F_2(\tilde{\mathbf{x}}_a^{(\ell)}) \\ \dots \\ c \frac{(\eta_M - \eta_1)}{2\pi\Delta} - F_M(\tilde{\mathbf{x}}_a^{(\ell)}) \end{bmatrix}.$$

The estimated value of  $\mathbf{h}$  can thus be given as

$$\mathbf{h} = \left( \mathbf{G}(\tilde{\mathbf{x}}_a^{(\ell)})^T \mathbf{G}(\tilde{\mathbf{x}}_a^{(\ell)}) \right)^{-1} \mathbf{G}(\tilde{\mathbf{x}}_a^{(\ell)})^T \mathbf{b}(\tilde{\mathbf{x}}_a^{(\ell)}). \quad (13)$$

The estimated location of  $\mathbf{x}_a^{(\ell)}$  is then updated as

$$\tilde{\mathbf{x}}_a^{(\ell)} \leftarrow \tilde{\mathbf{x}}_a^{(\ell)} + \mathbf{h}. \quad (14)$$

By repeating the update procedure several times,  $\tilde{\mathbf{x}}_a^{(\ell)}$  converges to  $\mathbf{x}_a^{(\ell)}$ . Besides,  $\mathbf{x}_b^{(\ell)}$  can be derived in the same way, which helps locate the TV in Sec. III-D. Substituting  $\mathbf{x}_a^{(\ell)}$  into (9) leads to the accurate synchronization gap  $\sigma$ . Moreover, since the synchronization gap is not affected by the MVs, it helps the SV to judge whether the signals of different AOs, are from the same TV.

**Remark 1** (Initial Value Selection). The Gauss-Newton method sometimes converges to a local optimal point due to the wrong selection of the initial  $\tilde{\mathbf{x}}_a^{(\ell)}$  [29]. It is recommended to use the solution satisfying any three equations among (10) as its initial selection, of which the convergence of the global optimal is verified by simulation.

**Remark 2** (Synchronization with Phase Error). In the presence of significant channel noise, the system of the equations E4 does not hold. To overcome the difficulty, we formulate the following minimization problem:

$$\mathbf{h}^* = \arg \min_{\mathbf{h}} \left\| \mathbf{G}(\tilde{\mathbf{x}}_a^{(\ell)}) \mathbf{h} - \mathbf{b}(\tilde{\mathbf{x}}_a^{(\ell)}) \right\|$$

$$= \left( \mathbf{G}(\tilde{\mathbf{x}}_a^{(\ell)})^T \mathbf{G}(\tilde{\mathbf{x}}_a^{(\ell)}) \right)^{-1} \mathbf{G}(\tilde{\mathbf{x}}_a^{(\ell)})^T \mathbf{b}(\tilde{\mathbf{x}}_a^{(\ell)}), \quad (15)$$

which has the same structure as (13). Note that the resultant  $\sigma$  from (9) is differently calculated depending on the choice of the SV's antenna  $m$ , denoted by  $\sigma_m$ . Averaging these values gives the accurate estimate of  $\sigma$  such that  $\sigma = \sum_{m=1}^M \sigma_m$ .

3) *Performance Analysis*: Assuming that the phase error follows an *independent identically distributed* (i.i.d.) Gaussian distribution  $\varepsilon \sim \mathcal{N}(0, \sigma_z^2 \mathbf{I})$ , the following proposition is provided.

**Proposition 1** (Error Covariance). As the number of SV's antennas  $M$  becomes larger, the covariance matrix  $\text{cov}(\tilde{\mathbf{x}}_a^{(\ell)})$  scales with  $\frac{1}{M-1}$ .

*Proof*. See Appendix A.  $\square$

**Remark 3** (Effect of SV's Number of Antennas). The SV's number of antennas  $M$  represents to the spatial sampling rate on the receive aperture. Larger  $M$  enables to decrease the distortion level, yielding  $(M-1)$  times faster convergence.

### B. Image Retrieval

The synchronization gap  $\sigma$  can be removed by the preceding step, facilitating to solve E2 in the following. Recall the synchronized demodulation (8) enabling to express  $y_m^{\ell,k}$  as a 3D surface integral form as

$$y_m^{\ell,k} = \Gamma^{(\ell)} \int_{\mathbb{R}^3} \mathbf{l}_{\mathbf{x}^{(\ell)}} \exp\left(-j \frac{2\pi f_k}{c} \sqrt{(\mathbf{x}^{(\ell)} - \mathbf{p}_m)(\mathbf{x}^{(\ell)} - \mathbf{p}_m)^T}\right) d\mathbf{x}^{(\ell)}, \quad (16)$$

where  $\sqrt{(\mathbf{x}^{(\ell)} - \mathbf{p}_m)(\mathbf{x}^{(\ell)} - \mathbf{p}_m)^T}$  represents the Euclidean distance between point  $\mathbf{x}^{(\ell)}$  and the location of the SV's antenna  $m$ , denoted by  $\mathbf{p}_m = [x_m, y_m, z_0]$ .

Let  $\mathbf{f}_k = \begin{bmatrix} f_k^{(x)} \\ f_k^{(y)} \\ f_k^{(z)} \end{bmatrix}$  denote the vector of which the components represent the spatial frequencies to the corresponding directions, namely,  $f_k = \sqrt{\left(f_k^{(x)}\right)^2 + \left(f_k^{(y)}\right)^2 + \left(f_k^{(z)}\right)^2}$ . The spherical wave in (16) can be decomposed into an infinite superposition of plane waves by rewriting the exponential term in terms of  $\mathbf{f}_k$  as

$$y_m^{\ell,k} = \Gamma^{(\ell)} \int_{\mathbb{R}^3} \mathbf{l}_{\mathbf{x}^{(\ell)}} \left\{ \int_{\sqrt{\mathbf{f}_k \mathbf{f}_k^T = f_k}} \exp\left(-j \frac{2\pi}{c} \mathbf{f}_k (\mathbf{x}^{(\ell)} - \mathbf{p}_m)^T\right) d\mathbf{f}_k \right\} d\mathbf{x}^{(\ell)}, \quad (17)$$

which is proved in [30] without approximation.

According to (17), the received signals can be rewritten with Fourier and inverse Fourier transform on  $\mathbf{x}^{(\ell)}$  and  $\mathbf{f}_k$ , respectively. With such relation between the transmit antenna location and the received data, the image  $\mathbf{l}_{\mathbf{x}^{(\ell)}}$  of VP  $\ell$  can be straightforward obtained from  $y_m^{\ell,k}$ , which is given as follows.

$$\tilde{\mathbf{l}}_{\mathbf{x}^{(\ell)}} = \text{FT}_{3\text{D}}^{-1} \left\{ \frac{\text{FT}_{2\text{D}} \left( \{y_m^{\ell,k}\}_{m=1}^M, f_k^{(x)}, f_k^{(y)} \right)}{\Gamma^{(\ell)}} \times \exp\left(-j \frac{2\pi}{c} \underbrace{\sqrt{(f_k)^2 - \left(f_k^{(x)}\right)^2 - \left(f_k^{(y)}\right)^2}}_{f_k^{(z)}} z_0 \right), \mathbf{x}^{(\ell)} \right\}, \quad (18)$$

where  $\text{FT}_{3\text{D}}^{-1}$ ,  $\text{FT}_{2\text{D}}$  represent 3-D inverse Fourier transform and 2-D Fourier transforms, respectively. Note that due to the finite and discrete deployment of antennas at both the TV and SV, discrete Fourier transform and inverse discrete Fourier

transform are used, and the estimated  $\tilde{l}_{\mathbf{x}^{(\ell)}}$  is a continuous value between  $[0, 1]$ . It is thus necessary to map  $\tilde{l}_{\mathbf{x}^{(\ell)}}$  into either one or zero, namely,

$$l_{\mathbf{x}^{(\ell)}} = \begin{cases} 1, & \text{if } |\tilde{l}_{\mathbf{x}^{(\ell)}}| \geq \nu, \\ 0, & \text{otherwise,} \end{cases} \quad \mathbf{x}^{(\ell)} \in \mathbb{R}^3 \quad (19)$$

where  $\nu$  represents the detection threshold.

**Remark 4 (Resampling).** To calculate the inverse 3D Fourier transform in (18), sampling on frequency domain with constant interval is necessary. However, due to the nonlinear relation of each frequency component as  $\sqrt{f_k \mathbf{f}_k^T} = f_k$ , regular samplings on  $f_k^{(x)}$  and  $f_k^{(y)}$  lead to the irregular sequence on  $f_k^{(z)}$  domain. It is thus required to make the sequence regular by using an interpolation, which is called a *resampling*. We use a linear interpolation for the resampling whose error is marginal verified by simulation.

### C. Resolution Analysis

In this subsection, we provide analysis on resolution of the multi-point position recovered by the above algorithm.

The direct relation between bandwidth  $\mathcal{B}$  and resolution  $\delta$  is established as  $\delta = \frac{c}{\mathcal{B}}$ , where  $c$  is the light speed. Based on this relation, azimuth and range resolutions are analyzed here.

1) *Azimuth Resolution:* Consider frequency  $f_k$ . The bandwidth in  $f^{(y)}$  direction, denoted by  $\mathcal{B}_y$  is approximately

$$\mathcal{B}_y \approx \mathbb{E}_k \left[ \frac{2D}{\sqrt{R^2 + D^2}} f_k \right] = \frac{2D}{\sqrt{R^2 + D^2}} f_c, \quad (20)$$

where  $f_c = \frac{f_1 + f_K}{2}$ ,  $R$  is the aperture size and  $D$  is the range. The azimuth resolution in  $Y$  direction can be straightforwardly obtained as

$$\delta_y \approx \frac{c\sqrt{R^2 + D^2}}{2f_c D}. \quad (21)$$

2) *Range Resolution:* The bandwidth in  $f_z$  direction is  $\mathcal{B}_z \approx (f_K - f_1)$ , and the range resolution is

$$\delta_z \approx \frac{c}{(f_K - f_1)}. \quad (22)$$

**Remark 5 (Sampling Requirements).** To achieve the above resolutions, there exist two kinds of sampling requirements.

**Spatial Sampling:** To achieve the resolution in (21), the receive antennas deployment needs to meet the Nyquist sampling criterion. Therefore, the distances between two adjacent receive antennas along  $X$  or  $Y$  directions are

$$\Delta_x = \Delta_y \leq \min \left\{ \frac{c}{2f_c} \frac{\sqrt{R^2 + D^2}}{D} \right\} \stackrel{(a)}{=} \frac{c}{2f_c}, \quad (23)$$

where (a) follows for the worst case with  $R = 0$ .

**Frequency sampling:** The frequency sampling interval refers to the minimum frequency gap  $\Delta$  to achieve the resolution  $\delta_z$  (22), given as  $\Delta \leq \frac{c}{R_{\max}}$ .

### D. Multi-Path Position Mapping

In this subsection, we aim at reconstructing the TV's RP using multiple VPs by solving E3 under the assumption that the reflection surfaces are vertical to the ground, which is common in practice. To this end, we use the representative points derived in Sec. III-A whose coordinates are  $\mathbf{x}_a^{(\ell)} = (x_a^{(\ell)}, y_a^{(\ell)}, z_a^{(\ell)})$  and  $\mathbf{x}_b^{(\ell)} = (x_b^{(\ell)}, y_b^{(\ell)}, z_b^{(\ell)})$ , which have geographical relations with the counterpart points on the RP denoted by  $\mathbf{x}_a = (x_a, y_a, z_a)$  and  $\mathbf{x}_b = (x_b, y_b, z_b)$  summarized in Lemma 1. Using the properties, the feasible condition of RP reconstruction is derived and the corresponding algorithm is designed based on the feasible condition.

**Lemma 1.** Consider VPs  $\ell_1$  and  $\ell_2$  whose representative points are  $\{\mathbf{x}_a^{(\ell_1)}, \mathbf{x}_b^{(\ell_1)}\}$  and  $\{\mathbf{x}_a^{(\ell_2)}, \mathbf{x}_b^{(\ell_2)}\}$  respectively, which have relations with the counterpart points of the real position denoted by  $(\mathbf{x}_a, \mathbf{x}_b)$  as follows.

- 1) Let  $\theta_\ell$  denote the directed angle from the  $X$ -axis (SV's moving direction) to the virtual line between  $\mathbf{x}_a^{(\ell)}$  and  $\mathbf{x}_a$  or  $\mathbf{x}_b^{(\ell)}$  and  $\mathbf{x}_b$  (see Fig. 2). The relation between  $\mathbf{x}_a$  is given in terms of  $\theta_{\ell_1}$  and  $\theta_{\ell_2}$  as

$$\begin{pmatrix} x_a \\ y_a \\ z_a \end{pmatrix} = \begin{pmatrix} \frac{(z_a^{(\ell_1)} - z_a^{(\ell_2)}) + (x_a^{(\ell_2)} \tan(\theta_{\ell_2}) - x_a^{(\ell_1)} \tan(\theta_{\ell_1}))}{\theta_{\ell_2} - \theta_{\ell_1}} \\ y_a^{(\ell_1)} \text{ or } y_a^{(\ell_2)} \\ z_a^{(\ell_1)} + \tan(\theta_{\ell_1}) (x_a - x_a^{(\ell_1)}) \end{pmatrix}, \quad (24)$$

and the relation between  $\mathbf{x}_b$  is given in terms of  $\theta_{\ell_1}$ , and  $\theta_{\ell_2}$  is obtained by replacing all  $a$  in (24) with  $b$ .

- 2) Let  $\phi_\ell$  denote the directed angle from the  $X$ -axis to the line segment of VP  $\ell$  as shown in Fig. 2. The angles  $\theta_\ell$  and  $\phi_\ell$  enable to make a relation between two VPs  $\ell_1$  and  $\ell_2$  as

$$\theta_{\ell_1} - \theta_{\ell_2} = \frac{\phi_{\ell_1} - \phi_{\ell_2}}{2}. \quad (25)$$

*Proof.* See Appendix B.  $\square$

Some intuitions are made from Lemma 1. First, it is shown in (24) that the coordinates of  $(\mathbf{x}_a, \mathbf{x}_b)$  can be calculated when  $\theta_{\ell_1}$  and  $\theta_{\ell_2}$  are given. Second, noting that  $\phi_{\ell_1}$  and  $\phi_{\ell_2}$  are observable from VPs  $\ell_1$  and  $\ell_2$  directly,  $\theta_{\ell_2}$  is easily calculated when  $\theta_{\ell_1}$  is given. Last,  $\theta_{\ell_1}$  and the resultant  $(\mathbf{x}_a, \mathbf{x}_b)$  are said to be correct if another combination of two VPs, for example  $\ell_1$  and  $\ell_3$ , can yield the equivalent result of  $(\mathbf{x}_a, \mathbf{x}_b)$ . As a result, we can lead to the following feasibility condition.

Based on Lemma 1 and Proposition ??, the representative points  $(\mathbf{x}_a, \mathbf{x}_b)$  are estimated as follows. Consider the angle  $\theta_1$  is given. According to (25), the other angles  $\{\theta_\ell\}_{\ell=2}^L$  is then expressed in terms of  $\theta_1$  as  $\theta_\ell = \theta_1 + \frac{\phi_\ell - \phi_1}{2}$ . By plugging one pair of  $(\theta_1, \theta_\ell)$  into (24), we can calculate the corresponding location of two representative points  $a$  and  $b$ , denoted by  $(z_a^{(\ell)}, z_b^{(\ell)})$ , which is equal to  $(\mathbf{x}_a, \mathbf{x}_b)$  when the given angle  $\theta_1$  is correct. In other words, estimating  $(\mathbf{x}_a, \mathbf{x}_b)$  is translated

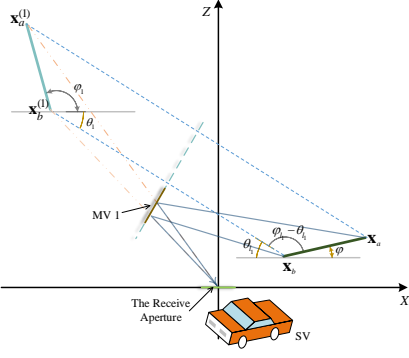


Figure 2: Relations between VPs and the TV.

into finding  $\theta_1$  minimizing the following squared Euclidean distance as

$$\theta_1^* = \arg \min_{\theta_1} \sum_{p=2}^L \sum_{q=2}^L \left( \left\| \mathbf{z}_a^{(q)} - \mathbf{z}_a^{(p)} \right\| + \left\| \mathbf{z}_b^{(q)} - \mathbf{z}_b^{(p)} \right\| \right) \quad (\text{E5})$$

where  $\mathbf{x}_a^* = \frac{1}{L-1} \sum_{\ell=2}^L \mathbf{z}_a^{(\ell)}$  and  $\mathbf{x}_b^* = \frac{1}{L-1} \sum_{\ell=2}^L \mathbf{z}_b^{(\ell)}$ . The optimal  $\theta_1^*$  is estimated by 1D search over  $[-\pi, \pi]$ , and the resultant  $(\mathbf{x}_a^*, \mathbf{x}_b^*)$  corresponds to the optimal  $(\mathbf{x}_a, \mathbf{x}_b)$ . Note that in case without phase error, the optimal solution of the problem E5 is zero and  $(\mathbf{x}_a^*, \mathbf{x}_b^*) = (\mathbf{x}_a, \mathbf{x}_b)$ .

**Remark 6** (Existence of LoS path). The LoS case is a special realization of NLoS case, where one couple of representative points  $(\mathbf{x}_a^{(0)}, \mathbf{x}_b^{(0)})$  are equivalent to the exact location  $(\mathbf{x}_a, \mathbf{x}_b)$ . Therefore, all mathematical expression for position mapping still holds in the LoS condition, and the resultant  $(\mathbf{x}_a^*, \mathbf{x}_b^*)$  can be obtained in the same way.

From the estimated  $\theta_\ell^*$  and  $\mathbf{x}_a^*$  (or  $\mathbf{x}_b^*$ ), the real position  $\{l_{\mathbf{x}}\}$  can be obtained by shifting the MI  $\ell$ ,  $\{l_{\mathbf{x}^{(\ell)}}\}$ . The reflection plane  $\ell$ , which is located on the middle of  $\mathbf{x}_a^*$  and  $\mathbf{x}_a^{(\ell)}$ , can be expressed by a line because it is perpendicular to  $X - Y$  plane such that

$$z = -\frac{1}{\tan(\theta_\ell^*)} \left( x - \frac{x_a^{(\ell)} + x_a^*}{2} \right) + \frac{(z_a^{(\ell)} + z_a^*)}{2}, \quad (26)$$

where  $\mathbf{x}_a^* = (x_a^*, y_a^*, z_a^*)$ . It is worth noting that the line (26) passes the middle points of all lines between the real points  $\mathbf{x}$  and virtual points  $\mathbf{x}^{(\ell)}$ , leading to the following mapping rule.

**Proposition 2** (Position Mapping). Consider the VP  $\ell$  represented by  $\{l_{\mathbf{x}^{(\ell)}}\}$ . Given  $\theta_\ell$  and  $\mathbf{x}_a^*$  (or  $\mathbf{x}_b^*$ ), the RP of the TV  $\{l_{\mathbf{x}^{(\ell)}}\}$  can be obtained by the following mapping function:

$$l_{\mathbf{x}} = l_{\mathbf{G}(\mathbf{x}^{(\ell)})}, \quad \mathbf{G}(\mathbf{x}^{(\ell)}) = \begin{pmatrix} x^* \\ y^* \\ z^* \end{pmatrix} \quad (27)$$

where

$$\begin{cases} x^* = x^{(\ell)} + \frac{(1 + \tan^2(\theta_\ell^*))}{\tan(\theta_\ell^*)} \left( \frac{x_a^{(\ell)} + x_a^*}{\tan(\theta_\ell^*)} + z_a^{(\ell)} + z_a^* - \frac{2x^{(\ell)}}{\tan(\theta_\ell^*)} - 2z^{(\ell)} \right) \\ y^* = y^{(\ell)} \\ z^* = z^{(\ell)} + (1 + \tan^2(\theta_\ell^*)) \left( \frac{x_a^{(\ell)} + x_a^* - 2x^{(\ell)}}{\tan(\theta_\ell^*)} + z_a^{(\ell)} + z_a^* - 2z^{(\ell)} \right) \end{cases}$$

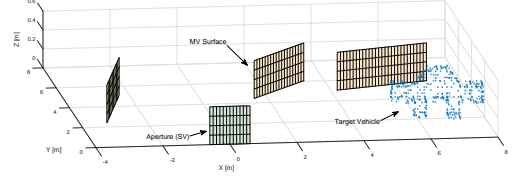


Figure 3: Initial topology.

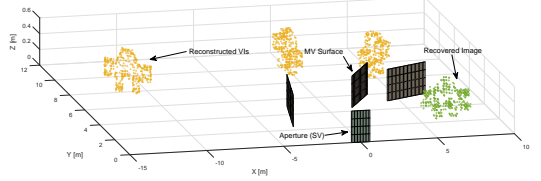


Figure 4: The detection of the VPs.

*Proof.* See Appendix D.  $\square$

#### IV. SIMULATION RESULTS

In this section, the performance of the proposed multi-point vehicular positioning techniques are evaluated by realistic settings. SW at 2 frequencies are used for the synchronization procedure. The number of frequencies used in the SFCW  $s(t)$  (1) is  $K = 512$  in  $57 \sim 60$  GHz with the constant gap  $\Delta = 5.86$  MHz. The two frequencies used in the SWs  $s_a(t)$  are  $(57 - \Delta \cdot i)$  GHz where  $i = 1, 2$ . The numbers of the TV's antennas  $N$  is 200 and the number of SV's antennas  $M$  is 256, uniformly deployed on the receive aperture with size  $1 \times 1$  m<sup>2</sup>. SNR of each received signal is fixed to 10 dB. For the performance metric, we use the Hausdorff distances defined as follows.

**Definition 1** (Hausdorff distance [34]). Consider two images  $\mathcal{A}$  and  $\mathcal{B}$ . The Hausdorff distance is defined as

$$H(\mathcal{A}, \mathcal{B}) = \max(h(\mathcal{A}, \mathcal{B}), h(\mathcal{B}, \mathcal{A})), \quad (28)$$

where  $h(\mathcal{A}, \mathcal{B}) = \max_{a \in \mathcal{A}} \min_{b \in \mathcal{B}} \|a - b\|$  is the direct Hausdorff distance from  $\mathcal{B}$  to  $\mathcal{A}$ .

##### A. Graphical Example of Multi-Point Positioning

This subsection aims at explaining the entire vehicular positioning procedure with graphical examples. Fig. 3(a) shows the original shape of the TV with the size  $3 \times 1 \times 0.6$  m<sup>3</sup>. We consider the topology with three MVs illustrated in Fig. 3(b). The X, Y, Z-axes are the SV's moving direction, height and depth, respectively. The TV is represented by discrete points, each of which is one TV's antenna. The receive aperture is parallel to Y-axis and located on (0, 0, 0). The equations of three MVs are  $z = 1.02x + 3$ ,  $z = \frac{x+13}{4}$ , and  $z = 3x + 4$ .

Using the MVs, the SV detects three VPs represented by yellow slots in Fig. 4, each of which is differentiable using AoA information. By the mapping algorithm in Proposition 2, each VP can be shifted to its real location represented by green spots with Hausdorff distance and direct Hausdorff distance

0.355m and 0.143 m respectively, relatively small compared to the size of the TV. The final detected position is obtained as in Fig. 5(b), similar to the original one in Fig. 5(a).

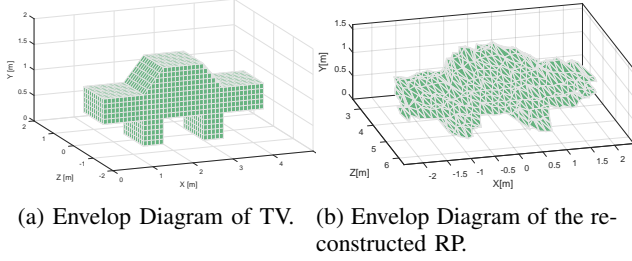


Figure 5: The envelop digram comparison of the TV model and the detected position.

### B. Effect of Distance between SV and TV

In Fig. 6, the Hausdorff distances are given under different TV-SV distances, showing that the positioning quality is degraded as the distance increases. This phenomenon can be explained by (21), where the spatial resolution becomes poor when the detection range  $R$  is large. Thus the SV may not be able to capture the clear position of the TVs far away, especially when the number of MVs is small. Moreover, the relation between the Hausdorff distance and the TV-SV distance is nonlinear. With noise in consideration, the Hausdorff distances increase faster when the TV-SV distance becomes larger.

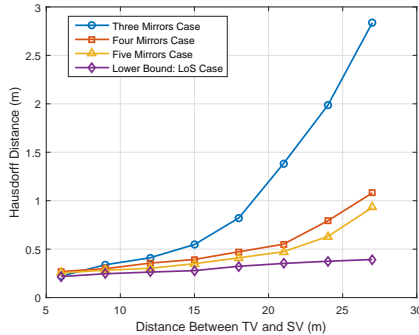


Figure 6: The performance of multi-point positioning versus distance.

### C. Effect of Mirror Vehicle Number

The relation between the performance and the number of MVs is also presented in Fig. 6. Signals reflected from any three MVs give one estimation of  $\theta_1$ , but the resultant positioning quality is low due to phase error. Larger  $L$  provides more combinations to estimate  $\theta_1$ , providing more accurate estimation of  $\theta_1$  by canceling out individual estimated error. The LoS case is considered as a lower bound because the operation in Sec. III-D is not involved.

## V. CONCLUSION

In this paper, a novel multi-point vehicular positioning approach via mmWave signal transmissions has been proposed to capture the shape and location information of the TVs in both LoS and NLoS. The synchronization issue has been well addressed by a novel PDoA-based hyperbolic positioning approach. The predictable reflections of mmWave frequency on the surface of vehicles have been exploited to form the geometry relation for obtaining the RP from multiple VPs. Existing vehicular positioning techniques relies on the LoS path while the proposed techniques overcome such limitations and opens a new area of mmWave-based vehicular positioning. We believe the proposed technique enables more intelligent and safer autonomous driving and the potential of mmWave-based sensing can still be activated in the future.

## APPENDIX

### A. Proof of proposition 1

Due to the assumption of Gaussian phase error, the covariance of the location estimation can be expressed as

$$\text{cov}(\tilde{\mathbf{x}}_a) = \mathbf{X} \sigma_z^2 \mathbf{I}_3, \quad (29)$$

where  $\mathbf{X}$  is a 3-by-3 matrix as

$$\begin{aligned} \mathbf{X} &= \left( \mathbf{G}(\tilde{\mathbf{x}}_a)^T \mathbf{G}(\tilde{\mathbf{x}}_a) \right)^{-1} = \left( \sum_{m=2}^M T_m(\tilde{\mathbf{x}}_a) \right)^{-1} \\ &= \left( \sum_{m=2}^M \begin{bmatrix} \left( \frac{\partial F_m(\tilde{\mathbf{x}}_a)}{\partial x_a} \right)^2 & \frac{\partial F_m(\tilde{\mathbf{x}}_a)}{\partial x_a} \frac{\partial F_m(\tilde{\mathbf{x}}_a)}{\partial y_a} & \frac{\partial F_m(\tilde{\mathbf{x}}_a)}{\partial x_a} \frac{\partial F_m(\tilde{\mathbf{x}}_a)}{\partial z_a} \\ \frac{\partial F_m(\tilde{\mathbf{x}}_a)}{\partial x_a} \frac{\partial F_m(\tilde{\mathbf{x}}_a)}{\partial y_a} & \left( \frac{\partial F_m(\tilde{\mathbf{x}}_a)}{\partial y_a} \right)^2 & \frac{\partial F_m(\tilde{\mathbf{x}}_a)}{\partial y_a} \frac{\partial F_m(\tilde{\mathbf{x}}_a)}{\partial z_a} \\ \frac{\partial F_m(\tilde{\mathbf{x}}_a)}{\partial x_a} \frac{\partial F_m(\tilde{\mathbf{x}}_a)}{\partial z_a} & \frac{\partial F_m(\tilde{\mathbf{x}}_a)}{\partial y_a} \frac{\partial F_m(\tilde{\mathbf{x}}_a)}{\partial z_a} & \left( \frac{\partial F_m(\tilde{\mathbf{x}}_a)}{\partial z_a} \right)^2 \end{bmatrix} \right)^{-1} \\ &= \frac{1}{M-1} \left( \frac{1}{M-1} \sum_{m=2}^M T_m(\tilde{\mathbf{x}}_a) \right)^{-1}, \quad (30) \end{aligned}$$

where the inverse matrix's each component converges to its expectation as  $M$  becomes large, which becomes independent to  $M$ . In other words,  $\mathbf{X}$  is inversely proportional to  $(M-1)$ , completing the proof.

### B. Proof of Lemma 1

In Fig. 7, we have  $\theta^{(\ell_1)} \in [-\pi, \pi]$  and the equations of line  $l_{\mathbf{x}_a^{(\ell_1)} \mathbf{x}_a}$  and  $l_{\mathbf{x}_a^{(\ell_2)} \mathbf{x}_a}$  are

$$\begin{aligned} l_{\mathbf{x}_a^{(\ell_1)} \mathbf{x}_a} &: z = z_a^{(\ell_1)} + \tan \theta^{(\ell_1)} (x - x_a^{(\ell_1)}), \\ l_{\mathbf{x}_a^{(\ell_2)} \mathbf{x}_a} &: z = z_a^{(\ell_2)} + \tan \theta^{(\ell_2)} (x - x_a^{(\ell_2)}). \end{aligned}$$

Thus we have

$$x_a = \frac{\left( z_a^{(\ell_1)} - z_a^{(\ell_2)} \right) + \left( x_a^{(\ell_2)} \tan \theta^{(\ell_2)} - x_a^{(\ell_1)} \tan \theta^{(\ell_1)} \right)}{\tan \theta^{(\ell_2)} - \tan \theta^{(\ell_1)}}, \quad (31)$$

and

$$z_a = z_a^{(\ell_1)} + \tan \theta^{(\ell_1)} (x_a - x_a^{(\ell_1)}). \quad (32)$$

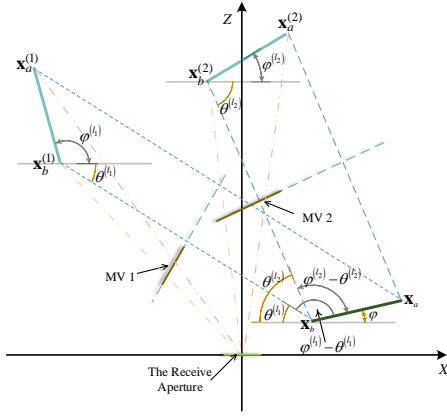


Figure 7: The geometry relations among different VPs and the TV.

The general relations in (24) can be derived similarly. Due to the symmetric relation between the VPs and the TV, we have

$$\pi - \varphi = \varphi^{(\ell_1)} - 2\theta^{(\ell_1)} = \varphi^{(\ell_2)} - 2\theta^{(\ell_2)}, \quad (33)$$

which can be observed from Fig. 7. Thus (25) is obtained.

### C. Proof of Proposition 2

Based on the line function of MV  $\ell$  surface (26), as well as the symmetric geometry relation between VP  $\ell$  and the TV, it is easy to establish the mathematical relation between  $\mathbf{x}^{(\ell)}$  and  $\mathbf{x}$  as

$$\begin{cases} x = x^{(\ell)} + \Delta x^{(\ell)} \\ z = z^{(\ell)} + \tan(\theta_\ell) \cdot \Delta x^{(\ell)} \end{cases}, \quad (34)$$

where  $\Delta x^{(\ell)}$  is the  $x$ -direction projection of distance between  $(x, z)$  and  $(x^{(\ell)}, z^{(\ell)})$ . The middle point of  $(x, z)$  and  $(x^{(\ell)}, z^{(\ell)})$  locates at the MV  $\ell$  surface with line function (26). Thus the middle point  $(x^{(\ell)} + \frac{\Delta x^{(\ell)}}{2}, z^{(\ell)} + \tan(\theta_\ell) \cdot \frac{\Delta x^{(\ell)}}{2})$  should satisfy function (26). Thus  $\Delta x^{(\ell)}$  can be solved by equation set expressed as

$$z_a^{(\ell)} + z_a - \frac{(x^{(\ell)} + \Delta x^{(\ell)} - x_a^{(\ell)} - x_a)}{\tan(\theta_\ell)} = z^{(\ell)} + \tan(\theta_\ell) \cdot \Delta x^{(\ell)}. \quad (35)$$

The result derived from (35) is given as

$$\Delta x^{(\ell)} = \left( \frac{1 + \tan^2(\theta_\ell^*)}{\tan(\theta_\ell^*)} \right) \left( \frac{x_a^{(\ell)} + x_a^* - 2x^{(\ell)}}{\tan(\theta_\ell^*)} + z_a^{(\ell)} + z_a^* - 2z^{(\ell)} \right). \quad (36)$$

Bring (36) into (34), the result (27) can be obtained straightforward by replacing  $(x, z)$  with the estimated value  $(x^*, z^*)$ . This finishes the proof.

## REFERENCES

[1] J. Choi, V. Va, N. Gonzalez-Prelcic, R. Daniels, C. R. Bhat, and R. W. Heath, "Millimeter-wave vehicular communication to support massive automotive sensing," *IEEE Communications Magazine*, vol. 54, pp. 160–167, December 2016.

[2] H. Wymeersch, G. Seco-Granados, G. Destino, D. Dardari, and F. Tufvesson, "5G mmWave positioning for vehicular networks," *IEEE Wireless Communications*, vol. 24, pp. 80–86, Dec 2017.

[3] K. Liu, H. B. Lim, E. Frazzoli, H. Ji, and V. C. S. Lee, "Improving positioning accuracy using gps pseudorange measurements for cooperative vehicular localization," *IEEE Transactions on Vehicular Technology*, vol. 63, pp. 2544–2556, July 2014.

[4] F. Gustafsson and F. Gunnarsson, "Mobile positioning using wireless networks: possibilities and fundamental limitations based on available wireless network measurements," *IEEE Signal Processing Magazine*, vol. 22, pp. 41–53, July 2005.

[5] W. Dai, Y. Shen, and M. Z. Win, "Distributed power allocation for cooperative wireless network localization," *IEEE Journal on Selected Areas in Communications*, vol. 33, pp. 28–40, Jan 2015.

[6] S. Gezici, G. B. Giannakis, H. Kobayashi, A. F. Molisch, H. V. Poor, and Z. Sahinoglu, "Localization via ultra-wideband radios: a look at positioning aspects for future sensor networks," *IEEE Signal Processing Magazine*, vol. 22, pp. 70–84, July 2005.

[7] K. Pahlavan, and J. P. Makela, "Indoor geolocation science and technology," *IEEE Communications Magazine*, vol. 40, pp. 112–118, Feb 2002.

[8] J. Shen, A. F. Molisch, and J. Salmi, "Accurate passive location estimation using toa measurements," *IEEE Transactions on Wireless Communications*, vol. 11, pp. 2182–2192, June 2012.

[9] S. Kong and B. Kim, "Error analysis of the odoa from the resolved first arrival path in lte," *IEEE Transactions on Wireless Communications*, vol. 15, pp. 6598–6610, Oct 2016.

[10] E. Uhlemann, "Time for autonomous vehicles to connect [connected vehicles]," *IEEE Vehicular Technology Magazine*, vol. 13, pp. 10–13, Sep. 2018.

[11] L. Yujiri, M. Shoucri, and P. Moffa, "Passive millimeter wave imaging," *IEEE Microwave Magazine*, vol. 4, pp. 39–50, Sept 2003.

[12] D. M. Sheen, D. L. McMakin, and T. E. Hall, "Three-dimensional millimeter-wave imaging for concealed weapon detection," *IEEE Transactions on Microwave Theory and Techniques*, vol. 49, pp. 1581–1592, Sep 2001.

[13] C. Nguyen and J. Park, *Stepped-Frequency Radar Sensors: Theory, Analysis and Design*. Springer International Publishing, 2016.

[14] R. K. Raney, H. Runge, R. Bamler, I. G. Cumming, and F. H. Wong, "Precision SAR processing using chirp scaling," *IEEE Transactions on Geoscience and Remote Sensing*, vol. 32, pp. 786–799, Jul 1994.

[15] X. Hu, N. Tong, Y. Zhang, and Y. Wang, "3d imaging using narrowband mimo radar and isar technique," in *2015 International Conference on Wireless Communications Signal Processing (WCSP)*, pp. 1–5, Oct 2015.

[16] S. S. Ahmed, A. Schiessl, F. Gumbmann, M. Tiebout, S. Methfessel, and L. Schmidt, "Advanced microwave imaging," *IEEE Microwave Magazine*, vol. 13, pp. 26–43, Sept 2012.

[17] H. V. Duong, M. A. Lefsky, T. Ramond, and C. Weimer, "The electronically steerable flash lidar: A full waveform scanning system for topographic and ecosystem structure applications," *IEEE Transactions on Geoscience and Remote Sensing*, vol. 50, pp. 4809–4820, Nov 2012.

[18] R. H. Rasshofer, M. Spies, and H. Spies, "Influences of weather phenomena on automotive laser radar systems," *Advances in Radio Science*, vol. 9, pp. 49–60, 2011.

[19] K. Han, S.-W. Ko, H. Chae, B.-H. Kim, and K. Huang, "Sensing Hidden Vehicles Based on Asynchronous V2V Transmission: A Multi-Path-Geometry Approach," *ArXiv e-prints*, Apr. 2018.

[20] F. Boccardi, R. W. Heath, A. Lozano, T. L. Marzetta, and P. Popovski, "Five disruptive technology directions for 5g," *IEEE Communications Magazine*, vol. 52, pp. 74–80, February 2014.

[21] Q. Cheng, A. Alomainy, and Y. Hao, "Near-field millimeter-wave phased array imaging with compressive sensing," *IEEE Access*, vol. 5, pp. 18975–18986, 2017.

[22] K. Sato, T. Manabe, T. Ihara, H. Saito, S. Ito, T. Tanaka, K. Sugai, N. Ohmi, Y. Murakami, M. Shibayama, Y. Konishi, and T. Kimura, "Measurements of reflection and transmission characteristics of interior structures of office building in the 60-GHz band," *IEEE Transactions on Antennas and Propagation*, vol. 45, pp. 1783–1792, Dec 1997.

[23] H. Zhao, R. Mayzus, S. Sun, M. Samimi, J. K. Schulz, Y. Azar, K. Wang, G. N. Wong, F. Gutierrez, and T. S. Rappaport, "28 GHz millimeter wave cellular communication measurements for reflection and penetration loss in and around buildings in new york city," in *2013 IEEE International Conference on Communications (ICC)*, pp. 5163–5167, June 2013.



- [24] D. Cohen, D. Cohen, Y. C. Eldar, and A. M. Haimovich, "Sub-Nyquist pulse doppler MIMO radar," in *2017 IEEE International Conference on Acoustics, Speech and Signal Processing (ICASSP)*, pp. 3201–3205, March 2017.
- [25] S. R. Saunders and S. R. Simon, *Antennas and Propagation for Wireless Communication Systems*. New York, NY, USA: John Wiley & Sons, Inc., 1st ed., 1999.
- [26] R. Yang, H. Li, L. Shiqiang, Z. Ping, T. Lulu, G. Xiangwu, and K. Xueyan, *High-Resolution Microwave Imaging*. Singapore: Springer Singapore, 2018.
- [27] O. Oshiga, S. Severi, and G. T. F. de Abreu, "Superresolution multipoint ranging with optimized sampling via orthogonally designed golomb rulers," vol. 15, pp. 267–282, Jan 2016.
- [28] H. Guo, K. Low, and H. Nguyen, "Optimizing the localization of a wireless sensor network in real time based on a low-cost microcontroller," *IEEE Transactions on Industrial Electronics*, vol. 58, pp. 741–749, March 2011.
- [29] W. Mascarenhas, "The divergence of the bfgs and gauss newton methods," *Mathematical Programming*, vol. 147, no. 1/2, pp. 253 – 276, 2014.
- [30] *Electromagnetic Wave Propagation, Radiation, and Scattering*. Wiley-Blackwell, 2017.
- [31] X. Zhuge and A. G. Yarovoy, "Three-dimensional near-field MIMO array imaging using range migration techniques," *IEEE Transactions on Image Processing*, vol. 21, pp. 3026–3033, June 2012.
- [32] M. I. Skolnik, *Introduction to radar systems /2nd edition/*, vol. -1. 01 1980.
- [33] D. Barrick, "Rough surface scattering based on the specular point theory," *IEEE Transactions on Antennas and Propagation*, vol. 16, pp. 449–454, July 1968.
- [34] D. P. Huttenlocher, G. A. Klanderman, and W. J. Rucklidge, "Comparing images using the Hausdorff distance," *IEEE Transactions on Pattern Analysis and Machine Intelligence*, vol. 15, pp. 850–863, Sep 1993.